Available online at www.sciencedirect.com

ScienceDirect

Procedia CIRP 108 (2022) 879–884

www.elsevier.com/locate/procedia

6th CIRP Conference on Surface Integrity

Ultrasonic assisted milling of a CoCrFeNi medium entropy alloy

Tim Richter[a]*, Diego Delgado Arroyo[a], Andreas Boerner[a], Dirk Schroepfer[a], Michael Rhode[a,b], Thomas Lindner[c], Martin Loebel[c], Bianca Preuß[c] and Thomas Lampke[c]

[a] *Bundesanstalt für Materialforschung und -prüfung (BAM), Unter den Eichen 87, Berlin 12205, Germany*
b Otto-von-Guericke University, Universitätsplatz 2, Magdeburg 39106, Germany
c Technical University Chemnitz, Straße der Nationen 62, Chemnitz 09111, Germany
* Corresponding author. Tel.: +493081044771. *E-mail address:* tim.richter@bam.de

Abstract

Medium and High Entropy Alloys (MEA/HEA) are recently developed material classes, providing manifold applications, e.g., due to extraordinary structural properties. In that connection, the machinability as important issue for the processing of these materials was not in the scientific focus. This study focusses on experimental analysis of milling process conditions including ultrasonic assisted milling (USAM) and their effects on the resulting surface integrity of equiatomic CoCrFeNi-MEA specimens. For that reason, milling parameters (cutting speed, feed per cutting edge) were systematically varied for both conventional milling and USAM. The surface integrity was analyzed in terms of topography, defects, and residual stresses. Especially USAM leads to a decrease of occurring cutting forces and, hence, to an improvement of the surface integrity. Beneficial effects were observed in terms of lower tensile residual stresses at high cutting speed and feed per cutting edge.

Keywords: medium entropy alloys; ultrasonic assisted milling; ball nose end milling

Nomenclature

C	direction dependent constant
D_t	milling tool diameter
F_r	resulting force
F_x	force in x-direction
F_y	force in y-direction
F_z	force in z-direction
f_z	feed per cutting edge
MEA/HEA	medium or high entropy alloy
n	rotational speed
R_z	average surface roughness
SPS	spark plasma sintering
USAM	ultrasonic assisted milling
v_c	cutting speed
λ	feed angle
τ	tilt angle
σ_{max}	maximal principal residual stress

1. Introduction

Since their introduction, the worldwide research interest in multi principal element alloys (MPEA), like medium-entropy alloys (MEA), has increased steadily [1, 2]. MEA are here defined as compositionally complex and disordered solid solutions containing two to four elements in near equiatomic proportions, while five or more different elements are referred to as high entropy alloys (HEA) [1]. Such MPEA are promising for a wide range of applications due to their outstanding properties (*e.g.*, high ductility combined with high strength) [1, 3, 4].

In that connection, a CoCrFeNi-MEA-system results from eliminating Mn from the well-known CoCrFeMnNi-HEA (or "Cantor" alloy) [5], in an attempt to increase its melting point and to improve both the strength and the corrosion resistance. Like the Cantor alloy, the CoCrFeNi system has a single-phase FCC columnar grain microstructure [6]. It shows excellent

10.1016/j.procir.2022.05.203

mechanical properties at cryogenic temperatures [7, 8], suggesting the use in components such as liquid gas storage tanks and piping. Typically, the HEA/MEA-systems are synthesized by casting [8], sintering [9, 10], as well as thermal spraying [11]. For the intended use as structural materials, there is still a big gap in scientific research regarding its necessary processability, e.g., machining is crucial for intermediate and finishing processes.

So far, research on the HEA/MEA-machinability is limited [12-17], with focus on the Cantor alloy. Gou et al. [12] conducted a study on different machining processes for CoCrFeMnNi, like milling, grinding, mechanical polishing, wire electro-discharge machining, and electro-polishing. In milled condition, the subsurface was highly affected, e.g., in terms of high microhardness and compressive residual stresses. Liborius et al. [15] investigated the influence of the tool material (CBN, PCD, CVD diamond and solid cemented carbide) and cutting speed (100–400 m/min) in face turning of spark plasma sintering (SPS) fabricated CoCrFeNi, reporting lowest roughness values and tool wear for CBN 90 tips at all cutting speeds. Litwa et al. [16] investigated the effect of depth of cut, feed per cutting edge and cutting speed, observing reduced cutting forces at low depth of cut and feed rate and at high cutting speeds for a CoCrFeMnNi HEA. They found a specific combination of feed rate and axial depth of cut to achieve a minimum surface roughness. For an intermediate depth of cut (~1.5 mm) R_a was maximal and increasing this parameter led to an increased process stability by lower tool deflection. These results are in accordance with those reported in [14, 17], that investigated ball nose end milling with ultrasonic assistance on the Cantor alloy at different feeds per cutting edge and cutting speeds. Groove defects are reported on the milled surface due to hard oxide particles. In that connection, the hybrid machining process USAM was characterized by improved machinability and surface integrity due to reduced occurring cutting forces compared to the conventional milling process.

Several studies have shown that USAM exhibits significant positive effects, i.e., reduced tool wear, lower cutting forces [18-22] and, hence, less surface defects, especially for hard-to-cut austenitic NiCr alloys, such as IN718. Fang et al. [18] observed a reduced surface defect formation (pits, bumps and gullies) for IN718 in case of low feed per cutting edge using USAM. Additionally, the formation of a built-up edge can be prevented and, for that reason, the three components of the cutting force. A reduction in cutting forces (12–25%) with USAM was obtained by Nath et al. [19], with a 12–14% reduced tool wear (expressed by a thinner and more even chip shape). Ahmed et al. [21] reported a reduced hardness for the subsurface layer in case of ultrasonic assisted turning.

The first results using USAM on HEA demonstrated, e.g., in [14, 17], due to the mechanical, structural, and chemical similarity to austenitic NiCr alloys are promising for machining of MEA. The intention of our present study is, hence, to evaluate for the first time the influence of contouring and finishing by means of ball nose end milling on the surface integrity and machinability of a SPS fabricated CoCrFeNi MEA. Consequently, the conventional process is compared to the USAM to investigate the MEA's applicability. Thus, the effect of ultrasonic assistance and processing parameters during milling and the resulting surface integrity will be the focus.

2. Experimental

2.1. Material preparation

In order to achieve a homogeneous element distribution, the powder feedstock material was produced by inert gas atomization using argon. A comprehensive characterization of the powders was carried out in [11, 23]. Dense compacts were produced using SPS (SPS KCE FCT-HP D 25-SI, FCT Systeme GmbH). The sintering temperature was set to 1050 °C, the heating rate to 100 K/min, and the uniaxial sintering pressure to 50 MPa. The holding time was 13 min. A graphite foil was applied as a release agent between the die walls and the powder. Argon was used as the process gas to avoid chemical reactions during the sintering process. Cooling of the specimens was carried out without control in the SPS system. The chemical composition measured by EDX is shown in Table 1. The ingots had a disk-like shape (40 mm diameter, 6 mm thickness). EDM was used to produce twelve rectangular samples with dimensions of 14x14x2 mm³ (length x width x thickness). As shown in Figure 1, EDX maps showed dark spots (upper left part) that were identified as Al-Ni rich and depleted in Cr and Fe.

Table 1: Chemical composition and hardness of CoCrFeNi MEA

at. %	Co	Cr	Fe	Ni	Al	HV0.5
Target	25	25	25	25	0	-
EDX	25.4	25.1	24.8	23.3	1.4	216

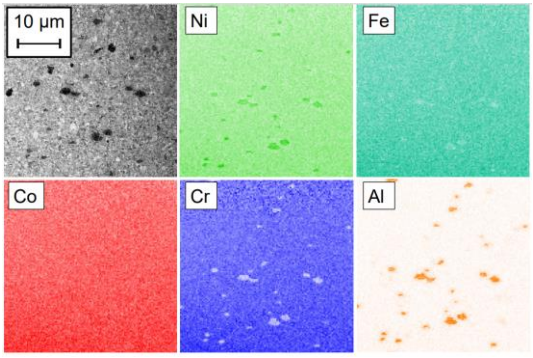

Figure 1: EDX mapping of the CoCrFeNi base material

2.2. Milling experiments

The dry milling experiments were carried out using a five-axis machine portal (DMG-Mori DMU65) modified for USAM. A right-hand ball nose end milling tool with four cutting edges was used according to DIN 6527L [24]. The tool, by WOLF Werkzeugtechnologie GmbH, was made of cemented carbide (tungsten carbide in cobalt matrix) and was coated by physical vapor deposition (PVD) with an AlTiCrN-layer (2 to 3 µm). It had a diameter of 6 mm, a relief angle of 15°, a helix angle of 30°, a rake angle of 4° and was designed for finish milling of hard to machine Ni-base alloys like IN718 (EN 2.4668). The tool inclination in x- (feed angle λ) and y- (tilt

angle τ) direction are fixed at 45°. The experimental setup is shown in more detail elsewhere [14, 17].

By varying the feed per cutting edge f_z (0.04 mm; 0.055 mm; 0.07 mm) and the cutting speed v_c (30 m/min; 70 m/min; 110 m/min) 12 milling experiments were carried out using a full factorial design of experiments, which is described in more detail in [14, 17]. These parameters were used instead of the rotational speed n and feed rate f for better comparability of different cutting processes. Due to the ball shaped tool v_c is not constant along the cutting edges. The rotational speed n is calculated via v_c and the feed λ and tilt angles τ, according to [25]. The USAM process (labeled as "100% USAM") was compared with the conventional milling (labeled as "0% USAM"). The design of experiments used, was already described in [14, 17]. The further parameters were constant: depth of cut (0.3 mm), step over (0.3 mm) and ultrasonic frequency (39.7 kHz). In each test approximately 59 mm³ of the material was removed. To avoid systematic errors due to machining heat, tool wear etc., the test order was established randomly, and central point tests were performed twice to examine the reproducibility. The first and last tests were performed with the same machining parameters to evaluate the influence of tool wear on the results.

2.3. Analysis

For in-situ force measurement in x-, y- and z-direction during the machining process, a Kistler dynamometer was used. The forces were measured with an incremental time of 0.02 ms. On each sample, 10 milling lines with 14 mm length were carried out. The resulting force F_r was calculated via equation 1 to improve the comparability of the individual tests:

$$\boldsymbol{F_r} = \sqrt{\boldsymbol{F_x}^2 + \boldsymbol{F_y}^2 + \boldsymbol{F_z}^2}. \quad (1)$$

Following Fr is the average of the maximum force of all cuts in an experiment. A detailed description of the force effect is given in [14, 17]. To elaborate the effect of the machining parameters (v_c, f_z and USAM) on F_r, a linear regression model was carried out using the open-source software R-studio .

To investigate the surface topography, the milled surfaces were examined by scanning electron microscopy (SEM, Phenom XL, Thermo Fisher Scientific) and light optical microscopy (LOM, Keyence VHX-7000). The roughness was measured in x- and y-directions with a contact profilometer (Hommel-Etamic T1000, Jenoptik) according to DIN EN ISO 4287 [26]. The measured R_z value was compared to the calculated theoretical roughness R_{zth}, according to [27]:

$$\boldsymbol{R_{tth}} = \boldsymbol{R_{zth}} = \frac{\boldsymbol{D_t}}{\boldsymbol{2}} - \sqrt{\frac{\boldsymbol{D_t^2} - \boldsymbol{C^2}}{\boldsymbol{4}}} \quad (2)$$

The theoretical maximum surface height R_{tth} is equal to the theoretical average surface roughness R_{zth} due to the same theoretical (index "th") roughness [26]. C is a constant depending on the direction and must be feed per cutting edge f_z (in feed direction x) or the step over (in normal feed direction y) and D_t is the tool diameter of the ball end mill.

For analyzing the mechanical influence of machining on the surface, residual stresses were measured by X-ray diffraction (XRD) with G3 Stresstech Goniometer using the sin² ψ method (parameters in Table 2). The residual stress were calculated using the elastic moduli for CoCrFeNi (Poisson's ratio ϑ = 0.25; Young's modulus E = 214 GPa), in accordance to [28].

Table 2: XRD-measurement parameters

XRD-measurement			
Measuring mode	sin² ψ	Collimator	3 mm
Radiation	Mn-Kα	Tube power	30 kV/ 6.7 mA
Detector	solid-state	ψ-tilting	0° to ±45°
Diffraction line	(311)	ψ-step	9
2Θ angel	156°	Measuring time	2 s

3. Results and discussion

3.1. Machining process

To characterize the cutting process the resulting forces F_r influenced by the cutting parameters are used. Figure 2 shows the contour plot of the linear regression model for F_r with an adjusted R^2 of 0.85 using the results of the f_z, v_c and ultrasonic assistance as parameters. Basically, the highest F_r are present at low v_c and high f_z (lower right corner) and decrease with increasing v_c and decreasing f_z (blue arrow). Feed per cutting edge is the most effective parameter, with larger feeds resulting in higher cutting forces, as expected according to the theory of cross-section of undeformed chip [29, 30]. Cutting speed also has a significant influence, with cutting forces decreasing at higher cutting speed. Finally, the effect of ultrasonic assistance (dashed lines) reduces the forces in all ranges of f_z and v_c by almost 2N (5–10 %). These results are comparable to those reported by Richter et al. on the Cantor alloy [17], and similarly exhibit the possibility to reduce cutting forces to almost the half value by increasing cutting speeds and lowering feed rates on the CoCrFeNi system.

3.2. Surface integrity

To characterize the surface integrity of the milled CoCrFeNi MEA, the influences of the machining processes on the topography (morphology and roughness) and the residual stresses (mechanical) are described below.

3.2.1. Topography

LOM and SEM images have been acquired and used to qualitatively describe the surface topography. Figure 3 shows 1x1 mm² images of the surface of the CoCrFeNi alloy after milling under the two extreme conditions of cutting speed and feed per cutting edge. Figures 3a and b show the lowest (v_c = 30 m/min and f_z = 0.04 mm) and c and d the highest values (v_c = 110 m/min and f_z = 0.07 mm) for conventional milling (a and c) and USAM respectively (b and d).

Ball nose end milling causes a regular peak-valley pattern in the feed direction. Feed per cutting edge is the most effective parameter on the surface topography, with larger f_z leading to larger peak-to-peak and peak-valley distances. The use of

USAM results in a wavy pattern on the surface (US pattern) as described in [14, 17], cf. Figure 3d. Since the frequency of vibration is constant, this pattern is finer at lower cutting speeds (Figure 3 b) and less visible using LOM.

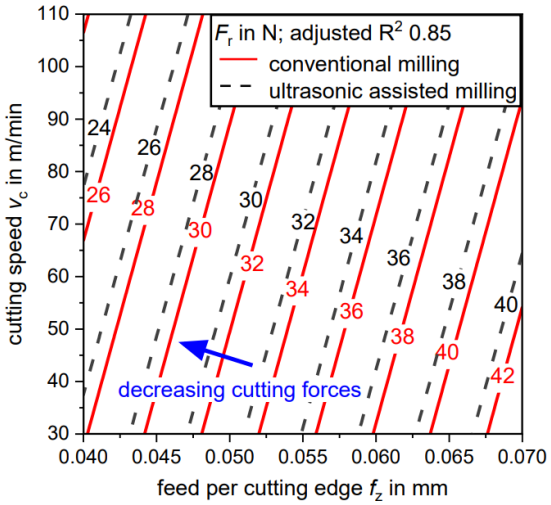

Figure 2: Linear regression model of the influence of cutting speed v_c, feed per cutting edge f_z and the ultrasonic assistance on the resulting force F_r from the results of the 12 machining experiments

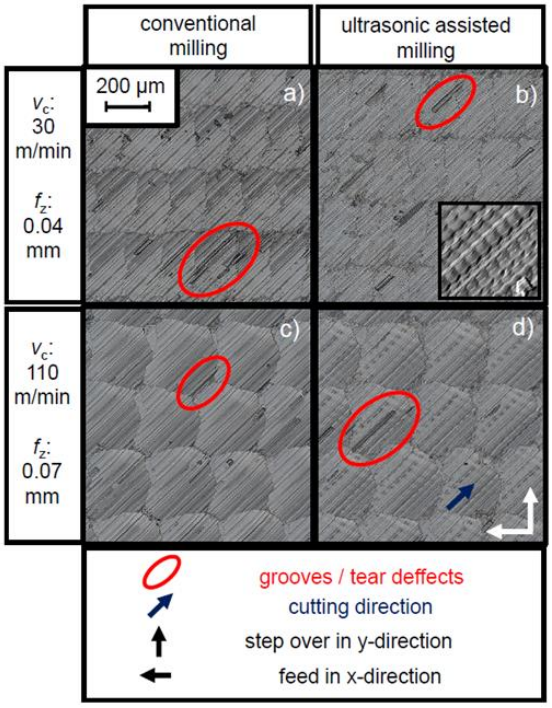

Figure 3: 1x1 mm light optical microscope images of the CoCrFeNi surface after conevntional milling with a) v_c= 30 m/min f_z= 0.04 mm; c) v_c = 110 m/min f_z= 0.07 mm and USAM with b) v_c= 30 m/min f_z= 0.04 mm; d) v_c = 110 m/min f_z= 0.07 mm

Figure 3 also shows the presence of grooves or tear defects, like reported in [17], which were also caused by hard oxide particles. These defects have been found for all cutting conditions. It remains unclarified, which cutting conditions are able to reduce them. The EDX analysis of a tear defect is shown in Figure 4. It can be assumed that they are caused by Al-Ni rich hard particles. Here, the tool edge encounters the hard particles breaking it and leaving an elongated tear defect with traits of the particle in the direction of tool edge movement. This mechanism of surface defect formation has been well described in [31]. For that reason it is reasonable that avoidance of defects like such (Al-rich) inclusions should contribute to an improved surface integrity.

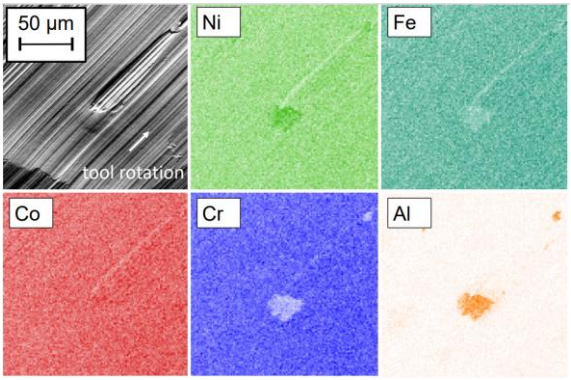

Figure 4: EDX-maps of a tear defect on the conventionally machined surface with v_c = 70 m/min and f_z = 0.055 mm

The average surface roughness parameter R_z is used to characterize the surface topography quantitatively. The resulting values depending on the cutting direction and parameters are shown in Figure 5. The most effective parameter on R_z measured in the feed direction (x), is feed per cutting edge. Higher feed rates lead to higher roughness values due to the larger distance between peaks and valleys. For R_z in *y*-direction no significant effect for f_z appears. This has been explained by the theoretical roughness R_{zth} prediction model by Nespor et al. [27], according to equation 2. The results in Figure 5b show the correlation between feed rate and roughness in the feed direction and stepover direction. Here, no influence of f_z in y-direction can be seen, whereas R_z in x-direction increases with increased f_z, the same tendency is also shown by the theoretical calculated roughness values R_{zth} from Table 3. However, the measured values are significantly higher than the theoretical ones (see Table 3) in the feed direction with: f_z = 0.04 mm, R_z ~ 2.5 µm; and for f_z = 0.07 mm, R_z ~ 4.5 µm respectively. In the stepover direction, the theoretical roughness, is only slightly lower than the measured values (~4–5 µm).

Table 3: Theoretical roughness R_{zth} in x- and y-direction influenced of different feed per cutting edges f_z

Feed per cutting edge f_z	R_{zth} in x – direction	R_{zth} in y – direction
0.04 mm	0.07 µm	3.75 µm
0.07 mm	0.20 µm	3.75 µm

This may be explained by non-ideal conditions of the cutting process due to tool deflection and vibrations in accordance to Nespor et al. [27]. Increasing tool vibrations due to cutting speed would also give reason for higher roughness values in both directions for higher cutting speed, cf. Figure 5a. Finally, USAM has a rather small and no significant effect on R_z, which may be accounted to the overall surface inhomogeneities, e.g., the presence of hard Al-Ni rich particles, and, therefore, a higher overall deviation of the R_z values.

3.2.2. Residual stresses

Milling affects the formation of residual stresses in the surface region, which were analyzed using XRD at the top surface (depth up to ~5 µm). From the determined residual stresses in 3 directions (0°, 45°, 90° to *x*-direction) the maximum principal stresses were calculated according to [22]. This maximum residual stresses σ_{max} for the CoCrFeNi MEA are shown in Figure 5c and d. They were in a range from 95 MPa to 180 MPa. The material yield strength is approx. 200 MPa according to [32]. Figure 5c displays the influence of the cutting speed v_c (30–110 m/min). The residual stresses increase with higher v_c for both the conventional and USAM processes. USAM reduces detrimental tensile residual stresses significantly compared to conventional milling at higher cutting speeds. At low cutting speeds, USAM shows no effect on the residual stress state.

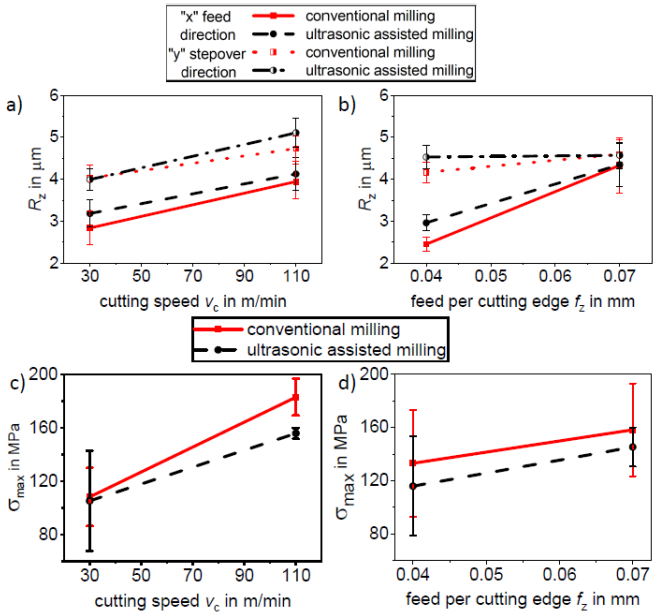

Figure 5: Influence of a) cutting speed v_c and b) feed per cutting edge f_z on roughness parameter R_z (average of 5 measurements with standard deviation) and Influence of c) cutting speed v_c (average of 0.04 and 0.07 mm for f_z with standard deviation) and d) feed per cutting edge f_z (average of 30 and 110 m/min for v_z with standard deviation) on the maximum principal residual stress σ_{max}

The influence of the feed per cutting edge f_z (0.04–0.07 mm) on the maximum principal residual stresses is shown in Figure 5d. Remarkably, the two processes show an increase of 10–20 MPa with increased f_z, but due to the high standard deviations, this trend cannot be considered significant. However, USAM causes a slight reduction of these, which may be traced back to a reduced work piece tool contact ratio with changed fracture dynamics [19] in connection with a reduction of the cutting forces compared to conventional milling according to [33], cf. Figure 2. Hence, it can be concluded that USAM is rather beneficial to avoid high tensile residual stresses especially for high feed rates and cutting speeds.

However, as shown in [17] no significant effect was observed for cutting speed v_c, feed rate f_z and ultrasonic assistance on the residual stress state at the surface of a cast CoCrFeMnNi HEA. Therefore, it is assumed that the altered influence of the milling conditions between the two fcc MPEA materials is due to the sintering process or the modified alloying.

4. Summary and conclusions

In this study, the machining and resulting surface integrity of a CoCrFeNi MEA were experimentally investigated for a conventional and an ultrasonic assisted ball nose end milling process. The cutting forces analysis tends to determine the machining process. The surface integrity is characterized by means of topography and residual stresses. From the results it can be concluded:

- The cutting forces decrease at lower feed rate, at higher cutting speed and for USAM
- Tear/groove defects due to Al-rich particles are present at all milled surfaces. Hence, no significant influence of USAM and cutting speed on the roughness parameter R_z was observed. A significant reduction of R_z only reveals for decreasing feed rate in feed direction.
- Increasing feed rate and cutting speed causes higher tensile residual stresses at the surface for conventional milling.
- USAM exhibits lower tensile residual stresses compared to conventional milling particularly for higher feed rates and cutting speeds.
- In terms of an appropriate surface integrity (low roughness and tensile residual stresses) for conventional milling process, lower cutting speed and feed rate should be considered. Thus, for a higher productivity with increased cutting speed and feed rate, USAM reveals a significant improvement in terms of surface integrity, especially with respect to surface residual stress state.

5. References

[1] D.B. Miracle, O.N. Senkov, A critical review of high entropy alloys and related concepts, Acta Materialia 122 (2017) 448-511.

[2] S. Gorsse, D.B. Miracle, O.N. Senkov, Mapping the world of complex concentrated alloys, Acta Materialia 135 (2017) 177-187.

[3] A.M. Manzoni, U. Glatzel, High-Entropy Alloys: Balancing Strength and Ductility at Room Temperature, Reference Module in Materials Science and Materials Engineering2020.

[4] E.P. George, W.A. Curtin, C.C. Tasan, High entropy alloys: A focused review of mechanical properties and deformation mechanisms, Acta Materialia 188 (2020) 435-474.

[5] B. Cantor, I.T.H. Chang, P. Knight, A.J.B. Vincent, Microstructural development in equiatomic multicomponent alloys, Materials Science and Engineering: A 375-377 (2004) 213-218.

[6] W.-R. Wang, W.-L. Wang, J.-W. Yeh, Phases, microstructure and mechanical properties of AlxCoCrFeNi high-entropy alloys at elevated temperatures, Journal of Alloys and Compounds 589 (2014) 143-152.

[7] Z. Wu, H. Bei, G.M. Pharr, E.P. George, Temperature

dependence of the mechanical properties of equiatomic solid solution alloys with face-centered cubic crystal structures, Acta Materialia 81 (2014) 428-441.
[8] J. Liu, X. Guo, Q. Lin, Z. He, X. An, L. Li, P.K. Liaw, X. Liao, L. Yu, J. Lin, L. Xie, J. Ren, Y. Zhang, Excellent ductility and serration feature of metastable CoCrFeNi high-entropy alloy at extremely low temperatures, Science China Materials 62(6) (2018) 853-863.
[9] R.B. Mane, B.B. Panigrahi, Sintering mechanisms of mechanically alloyed CoCrFeNi high-entropy alloy powders, Journal of Materials Research 33(19) (2018) 3321-3329.
[10] M.A. Hassan, I.M. Ghayad, A.S.A. Mohamed, A.E. El-Nikhaily, O.A. Elkady, Improvement ductility and corrosion resistance of CoCrFeNi and AlCoCrFeNi HEAs by electroless copper technique, Journal of Materials Research and Technology 13 (2021) 463-485.
[11] M. Löbel, T. Lindner, R. Hunger, R. Berger, T. Lampke, Precipitation Hardening of the HVOF Sprayed Single-Phase High-Entropy Alloy CrFeCoNi, Coatings 10(7) (2020).
[12] J. Guo, M. Goh, Z. Zhu, X. Lee, M.L.S. Nai, J. Wei, On the machining of selective laser melting CoCrFeMnNi high-entropy alloy, Materials & Design 153 (2018) 211-220.
[13] B. Clauß, H. Liborius, T. Lindner, M. Löbel, A. Schnubert, T. Lampke, Influence of the cutting parameters on the surface properties in turning of a thermally sprayed AlCoCrFeNiTi coating, 5th CIRP CSI 2020, Elsevier B.V., 2020.
[14] T. Richter, D. Schröpfer, M. Rhode, A. Börner, Influence of modern machining processes on the surface integrity of high-entropy alloys, Symposium on Materials and Joining Technology, IOP Publishing, 2020.
[15] H. Liborius, T. Uhlig, B. Clauß, A. Nestler, T. Lindner, A. Schubert, G. Wagner, T. Lampke, Influence of the cutting material on tool wear, surface roughness, and force components for different cutting speeds in face turning of CoCrFeNi high-entropy alloys, IOP Conference Series: Materials Science and Engineering 1147(1) (2021).
[16] P. Litwa, E. Hernandez-Nava, D. Guan, R. Goodall, K.K. Wika, The additive manufacture processing and machinability of CrMnFeCoNi high entropy alloy, Materials & Design 198 (2021).
[17] T. Richter, D. Schroepfer, M. Rhode, A. Boerner, R.S. Neumann, M. Schneider, G. Laplanche, Influence of machining on the surface integrity of high- and medium-entropy alloys, Materials Chemistry and Physics 275 (2022).
[18] B. Fang, Z. Yuan, D. Li, L. Gao, Effect of ultrasonic vibration on finished quality in ultrasonic vibration assisted micromilling of Inconel718, Chinese Journal of Aeronautics 34(6) (2021) 209-219.
[19] C. Nath, M. Rahman, Evaluation of ultrasonic vibration cutting while machining Inconel 718, Int J Precis Eng Man 9(2) (2008) 63-68.
[20] A. Suárez, F. Veiga, L.N.L. de Lacalle, R. Polvorosa, S. Lutze, A. Wretland, Effects of Ultrasonics-Assisted Face Milling on Surface Integrity and Fatigue Life of Ni-Alloy 718, Journal of Materials Engineering and Performance 25(11) (2016) 5076-5086.
[21] N. Ahmed, A.V. Mitrofanov, V.I. Babitsky, V.V. Silberschmidt, Analysis of material response to ultrasonic vibration loading in turning Inconel 718, Materials Science and Engineering: A 424(1-2) (2006) 318-325.
[22] D. Schroepfer, K. Treutler, A. Boerner, R. Gustus, T. Kannengiesser, V. Wesling, W. Maus-Friedrichs, Surface finishing of hard-to-machine cladding alloys for highly stressed components, The International Journal of Advanced Manufacturing Technology 114(5-6) (2021) 1427-1442.
[23] L.-M. Rymer, T. Lindner, P. Frint, M. Löbel, T. Lampke, Designing (Ultra)Fine-Grained High-Entropy Alloys by Spark Plasma Sintering and Equal-Channel Angular Pressing, Crystals 10(12) (2020).
[24] DIN-6527L, DIN-6527L, Vollhartmetall-Schaftfräser mit abgesetztem Zylinderschaft-Maße, Beuth publishing DIN, 2002.
[25] B. Denkena, D. Nespor, V. Böß, J. Köhler, Residual stresses formation after re-contouring of welded Ti-6Al-4V parts by means of 5-axis ball nose end milling, CIRP Journal of Manufacturing Science and Technology 7(4) (2014) 347-360.
[26] DIN EN ISO 4287, Geometrische Produktspezifikation (GPS) - Oberflächenbeschaffenheit: Tastschnittverfahren - Benennungen, Definitionen und Kenngrößen der Oberflächenbeschaffenheit, Beuth publishing DIN, 2010.
[27] D. Nespor, B. Denkena, T. Grove, O. Pape, Surface topography after re-contouring of welded Ti-6Al-4V parts by means of 5-axis ball nose end milling, The International Journal of Advanced Manufacturing Technology 85(5-8) (2015) 1585-1602.
[28] G. Laplanche, P. Gadaud, C. Bärsch, K. Demtröder, C. Reinhart, J. Schreuer, E.P. George, Elastic moduli and thermal expansion coefficients of medium-entropy subsystems of the CrMnFeCoNi high-entropy alloy, Journal of Alloys and Compounds 746 (2018) 244-255.
[29] J. Kundrák, C. Felhő, Investigation of the Topography of Face Milled Surfaces, Materials Science Forum 919 (2018) 78-83.
[30] J. Kundrák, B. Karpuschewski, Z. Pálmai, C. Felhő, T. Makkai, D. Borysenko, The energetic characteristics of milling with changing cross-section in the definition of specific cutting force by FEM method, CIRP Journal of Manufacturing Science and Technology 32 (2021) 61-69.
[31] C. Liu, C. Ren, G. Wang, Y. Yang, L. Zhang, Study on surface defects in milling Inconel 718 super alloy, Journal of Mechanical Science and Technology 29(4) (2015) 1723-1730.
[32] W. Huo, H. Zhou, F. Fang, X. Hu, Z. Xie, J. Jiang, Strain-rate effect upon the tensile behavior of CoCrFeNi high-entropy alloys, Materials Science and Engineering: A 689 (2017) 366-369.
[33] P. Zou, Y. Xu, Y. He, M. Chen, H. Wu, Experimental Investigation of Ultrasonic Vibration Assisted Turning of 304 Austenitic Stainless Steel, Shock and Vibration 2015 (2015) 1-19.